

UC San Diego

UC San Diego Previously Published Works

Title

Revised and updated paleomagnetic results from Costa Rica

Permalink

<https://escholarship.org/uc/item/1tm3h4dx>

Journal

Geochemistry Geophysics Geosystems, 14(9)

ISSN

1525-2027

Authors

Cromwell, G
Constable, CG
Staudigel, H
[et al.](#)

Publication Date

2013-09-01

DOI

10.1002/ggge.20199

Peer reviewed



Revised and updated paleomagnetic results from Costa Rica

G. Cromwell

Geosciences Research Division, Scripps Institution of Oceanography, University of California San Diego, 9500 Gilman Drive, La Jolla, California, 92093-0208, USA (gcromwell@ucsd.edu)

C. G. Constable and H. Staudigel

Institute of Geophysics and Planetary Physics, Scripps Institution of Oceanography, University of California, San Diego, La Jolla, California, USA

L. Tauxe

Geosciences Research Division, Scripps Institution of Oceanography, University of California, San Diego, La Jolla, California, USA

P. Gans

Department of Earth Science, University of California, Santa Barbara, California, USA

[1] Paleomagnetic results from globally distributed lava flows have been collected and analyzed under the time-averaged field initiative (TAFI), a multi-institutional collaboration started in 1996 and designed to improve the geographic and temporal coverage of the 0–5 Ma paleomagnetic database for studying both the time-averaged field and its very long-term secular variations. Paleomagnetic samples were collected from 35 volcanic units, either lava flows or ignimbrites, in Costa Rica in December 1998 and February 2000 from the Cordilleras Central and Guanacaste, the underlying Canas, Liberia and Bagaces formations and from Volcano Arenal. Age estimates range from approximately 40 ka to slightly over 6 Ma. Although initial results from these sites were used in a global synthesis of TAFI data by Johnson et al. (2008), a full description of methodology was not presented. This paper documents the definitive collection of results comprising 28 paleomagnetic directions (24 normal, 4 reversed), with enhanced precision and new geological interpretations, adding two paleointensity estimates and 19 correlated ⁴⁰Ar/³⁹Ar radiometric ages. The average field direction is consistent with that of a geocentric axial dipole and dispersion of virtual geomagnetic poles ($17.3 \pm 4.6^\circ$) is in general agreement with predictions from several statistical paleosecular variation models. Paleointensity estimates from two sites give an average field strength of 26.3 μ T and a virtual axial dipole moment of 65 ZAm². The definitive results provide a useful augmentation of the global database for the longer term goal of developing new statistical descriptions of paleomagnetic field behavior.

Components: 6,855 words, 4 figures, 3 tables.

Keywords: Costa Rica; paleosecular variation; paleointensity; TAFI.

Index Terms: 1522 Paleomagnetic secular variation: Geomagnetism and Paleomagnetism; 1521 Paleointensity: Geomagnetism and Paleomagnetism; 1599 General or miscellaneous: Geomagnetism and Paleomagnetism.

Received 12 March 2013; **Accepted** 7 June 2013; **Published** 3 September 2013.

Cromwell, G., C. G. Constable, H. Staudigel, L. Tauxe, and P. Gans (2013), Revised and updated paleomagnetic results from Costa Rica, *Geochem. Geophys. Geosyst.*, 14, 3379–3388, doi:10.1002/ggge.20199.



1. Introduction

[2] The behavior of the ancient geomagnetic field can be characterized by looking at discrete magnetic directions and intensities obtained from lava flows and sediments over the last 10^4 to 10^6 years. Volcanic rocks play an especially important role in determining the average structure and variability of the geomagnetic field, since the age of individual volcanic units can be determined using radiometric dating methods. Several global compilations of paleomagnetic directions from lava flows and thin dikes [e.g., *McElhinny and Merrill*, 1975; *Lee*, 1983; *Johnson et al.*, 2008] have been used to derive models of the time-averaged field (TAF) [e.g., *Johnson and Constable*, 1995; *McElhinny et al.*, 1996] and statistical descriptions of its paleosecular variation (PSV) [e.g., *Constable and Parker*, 1988; *Hulot and Le Mouél*, 1994; *McElhinny and McFadden*, 1997; *Tauxe and Kent*, 2004] for the time period 0–5 Ma.

[3] Accurate descriptions of geomagnetic field structures require global data sets of high-quality paleomagnetic data with good temporal distribution and spatial coverage. Most TAF and PSV models have focused on the past 5 My because the volume of accessible geological materials diminishes with age and the effects of plate motion are well documented for this time period. The global data compilations often suffer from limited geographical coverage, inadequate or poorly documented temporal sampling, or poor data quality. Sixteen years ago, *McElhinny and McFadden* [1997] reported that only 12% of directional sites (440 out of 3719) met the modern paleomagnetic laboratory standards defined as a demagnetization code (DC) of 4 by *McElhinny et al.* [1996]. In the mid-1990s, the multi-institutional time-averaged field initiative (TAFI) was developed to improve geographic and temporal coverage of the paleomagnetic database by expanding the existing data set and reexamining some paleomagnetic locations with modern laboratory methods.

[4] Costa Rica was an original target of the TAFI project because of the paucity of data from low-latitude and equatorial regions. Researchers at Scripps Institution of Oceanography (SIO) conducted two field trips to Costa Rica in 1998 and 2000, collecting samples from 35 lava flows. A table of preliminary directional results from Costa Rica was published by *Johnson et al.* [2008] as part of a compilation of TAFI data and other regional paleodirectional studies. However, there remained room for

improvement in the data quality. The results published in *Johnson et al.* [2008] are nearly complete in a paleomagnetic sense, but lack detail in the geologic interpretation of the sampled lava flows. Several sites from the initial Costa Rica results failed to pass site selection criteria set by *Johnson et al.* [2008], because of an insufficient number of successfully demagnetized samples per site ($n \geq 5$ was specified), or because of insufficient precision in the average site direction (a within site Fisher precision statistic of $k_w \geq 50$ was required). Many samples were not fully demagnetized and Thellier-Thellier experiments were incomplete or not performed on some sites. In this study, we improve the reliability of the results, performing additional paleodirectional and paleointensity experiments as needed, and bringing all previous experiments to completion. We ensured that all characteristic magnetization directions and intensities were interpreted in a consistent manner so that more sites are acceptable for later TAF and PSV analyses. We determined new geological interpretations for several lava flows and increased the overall number of statistically acceptable samples and sites.

[5] In the following sections, we present the geologic context for Costa Rica and our sampled lava flows, and we detail the experimental methods used for $^{40}\text{Ar}/^{39}\text{Ar}$ radiometric dating, paleodirections, and paleointensity. The main paleomagnetic outcomes do not change significantly from *Johnson et al.* [2008], but the Costa Rica data set is now comprehensive due to the methodology and interpretations presented in this manuscript.

2. Geology and Sampling

[6] Costa Rica lies between Nicaragua and Panama in the southern part of Central America (Figure 1), where volcanic activity has occurred over a broad area as the Central American volcanic arc (CAVA) evolved over at least the past 24 Ma. The magmatism has been strongly episodic and regionally variable in part related to the complicated subduction of the Cocos plate beneath the Caribbean plate. *Gans et al.* [2002] conducted a comprehensive field and $^{40}\text{Ar}/^{39}\text{Ar}$ investigation (more than 200 age determinations) of Neogene volcanism in Costa Rica and *MacMillan et al.* [2004] use these constraints to present the plate tectonic history since mid-Miocene for the southern CAVA. Numerous geophysical, petrographic, and geochemical [e.g., *Drummond et al.*, 1995; *Vogel*

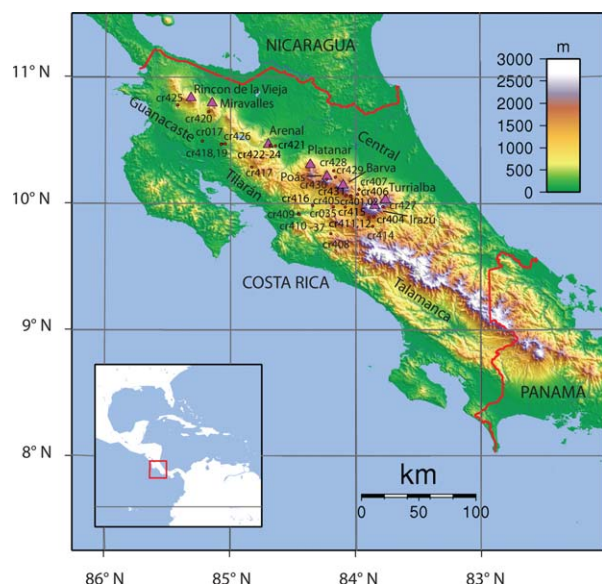


Figure 1. Topographic map of Costa Rica with all sampled site locations. Map modified from *Sadalmelik* [2007], elevations are in meters above sea level. Site locations are shown as red dots accompanied by site names. Costa Rica has four main mountain ranges and eight active volcanoes (marked as purple triangles). The Cordillera Guanacaste in the northwest includes the Rincon de la Vieja and Miravalles volcanoes. To the southeast is the Cordillera Tilarán and Arenal volcano, followed by the Cordillera Central which contains five volcanoes: Platanar, Poás, Barva, Turrialba, and Irazú. The Cordillera Talamanca is the largest mountain range, extending south into Panama.

et al., 2004; *Zimmer et al.*, 2004] studies have contributed to evolving views of the region, but prior to 1998 there was no paleomagnetic study of 0–5 Ma lava flows. The terrain in Costa Rica is dominated by the continental divide, with a series of mountain ranges (roughly from northwest to southeast they are Cordillera Guanacaste, Cordillera Tilarán, Cordillera Central, and the Cordillera Talamanca in the southern part of the country) separating the Pacific and Caribbean watersheds. Modern composite volcanoes (those active today include Rincon de la Vieja, Arenal, Platanar, Poás, Barva, Miravalles, Irazú, and Turrialba) have mainly been built during two recent peaks in volcanism (0.4–0.6 and <0.1 Ma) and are superimposed on older volcanic formations. Gabbro to granodiorite plutons exposed in three major ranges the Talamanca, Central, and Tilarán were emplaced from ~17 to 3.5 Ma, but mainly during 7–10 Ma an apparent gap in volcanism, and were not the primary target of our sampling.

[7] Aside from the general location the major attraction of Costa Rica for the TAFI project was

the ability to sample the paleomagnetic field across several million years of volcanic activity, ranging from Plio-Pleistocene to Holocene in age. We sampled 35 young volcanic sites, predominantly ignimbrites and andesitic lavas, from the Cordilleras Central, Tilarán, and Guanacaste, the underlying Canas, Liberia, and Bagaces formations and from Volcano Arenal. A minimum of 10 samples per site were collected with a portable gasoline powered drill. All were oriented with magnetic compass and sun compass whenever possible.

3. $^{40}\text{Ar}/^{39}\text{Ar}$ Dating and Sites Ages

[8] $^{40}\text{Ar}/^{39}\text{Ar}$ incremental heating experiments were performed at the UC Santa Barbara Argon Laboratory. Samples were crushed and sieved to 0.25–0.5 mm fraction and were then exposed to heavy duty ultrasonic treatment. Magnetic density separation and hand picking were performed to obtain pure groundmass. Unirradiated splits of most whole rock samples were first analyzed on the mass spectrometer to get a preliminary assessment of the age and expected radiogenic yields, and thus better plan the analytical strategy. More silicic units were first coarsely crushed and carefully hand picked to remove as much of the xenolithic contamination as possible.

[9] Depending on the age and potassium content, 20–400 mg of each sample was packaged for irradiation at the Oregon State research reactor. The samples were divided into a younger group (estimated <500 ka) that was given a 10 min irradiation and an older group that was irradiated for 40 min. All the samples were monitored using Taylor Creek Rhyolite sanidine (assigned age 27.92 Ma).

[10] Groundmass concentrates from mafic lavas tended to yield typical “recoil” type spectra, with old apparent ages in low temperature steps, but generally well defined plateaus for the gas released at 800–1000°C. Plagioclase from more silicic units generally gave fairly flat release spectra with well defined plateaus, except in cases with obvious xenocrystic contamination.

[11] $^{40}\text{Ar}/^{39}\text{Ar}$ incremental heating experiments were successful on 18 sites with ages ranging from 41 ka to 6.1 Ma (see Table 1). All 18 $^{40}\text{Ar}/^{39}\text{Ar}$ results are previously reported by *Pérez et al.* [2006] or *Alvarado and Gans* [2012]. An



Table 1. Costa Rica Directional Statistics^a

Site Name	Alt. Name	Age ^b (ka)	Lat (°N)	Lon (°E)	Dec	Inc	nl/np/nn (N)	k_w (k)	R	α_{95}	VGP Lat	VGP Lon
cr017 _y	CR-017	2110 ± 20 ⁽³⁾	10.4967	-85.2290	14.0	18.6	5/0/5	1008	4.9960	2.4	76.2	7.4
cr035 _x			9.9707	-84.1800	359.3	23.7	1/10/11	477	10.9895	2.3		
cr036 _y	CR-019	321 ± 18 ⁽²⁾	9.9707	-84.1798	353.7	23.6	3/3/6	142	5.9753	6.1	83.4	207.2
cr037 _x	CR-018	496 ± 16 ⁽³⁾	9.9707	-84.1800	357.9	27.9	11/0/11	106	10.9058	4.5	84.7	253.1
cr401 _x	CR-004	426 ± 14 ⁽³⁾	10.0592	-84.0393	347.2	-7.0	7/1/8	827	7.9921	1.9	71.4	139.8
cr402 _x	CR-006	427 ± 6 ⁽³⁾	10.0547	-84.0387	0.6	-18.1	6/0/6	131	5.9619	5.9	70.7	94.2
cr404 _y	CR-IZ-02-1	57 ± 13 ⁽¹⁾	9.8905	-83.8552	347.0	5.5	6/2/8	351	7.9829	3.0	75.2	158.1
cr405 _x	CR-021	332 ± 12 ⁽²⁾	9.9718	-84.1801	354.6	21.6	7/3/10	262	9.9714	3.0	84.6	199.3
cr406 _x	CR-230	400 ± 40 ⁽³⁾	10.0703	-83.9848	0.2	22.7	7/2/9	1469	8.9952	1.4	88.2	282.4
cr407 _x	CR-233	889 ± 12 ⁽³⁾	10.1103	-83.9745	219.5	25.0	10/0/10	233	9.9613	3.2	-44.4	215.9
cr408 _x	CR-038	270 ± 6 ⁽²⁾	9.7570	-84.1999	14.2	5.5	1/8/9	153	8.9739	4.6	74.3	31.3
cr409 _x	CR-039	330.7 ± 2 ⁽²⁾	9.9162	-84.4594	340.9	22.4	7/2/9	130	8.9499	4.6	71.2	192.6
cr410 _y			9.9147	-84.4435	351.0	24.3	7/2/9	81	8.9137	5.8	80.7	205.0
cr411 _x			9.8847	-83.8944	22.2	-16.7	7/2/9	343	8.9796	2.8	61.2	45.2
cr412 _y	CR-001	176 ± 2 ⁽³⁾	9.8847	-83.8944	28.8	-3.3	7/0/7	393	6.9847	3.0	59.1	26.5
cr414l			9.8156	-83.8633	358.6	-15.0	5/0/5	747	4.9946	2.8	72.5	100.8
cr414m			9.8156	-83.8633	66.1	15.3	4/1/5	27	4.8695	15.5		
cr414u			9.8156	-83.8633	13.1	-12.2	5/0/5	4850	4.9992	1.1	69.4	56.4
cr415 _x	CR-011	338 ± 4 ⁽²⁾	9.9692	-84.0849	359.1	10.5	7/0/7	249	6.9759	3.8	85.2	106.8
cr416 _y	CR-062	6100 ± 300 ⁽³⁾	9.9828	-84.3464	164.0	-6.5	2/0/2	8	1.8808	180.0		
cr417 _x	CR-169	1920 ± 40 ⁽³⁾	10.2889	-84.8336	23.1	37.4	6/0/6	83	5.9396	7.4	65.4	336.8
cr418 _x			10.4738	-85.0726	181.2	-8.4	11/0/11	752	10.9867	1.7	-83.6	264.1
cr419 _x			10.4710	-85.0748	354.1	34.3	5/1/6	80	5.9436	7.7	79.9	241.3
cr420 _x			10.7293	-85.1796	7.6	31.2	11/0/11	1040	10.9904	1.4	80.4	324.3
cr421 _x	CR-015	46 ± 6 ⁽³⁾	10.4578	-84.6432	347.2	41.9	2/3/5	14	4.8191	24.1		
cr422-423 _x			10.4608	-84.6851	348.7	32.8	14/2/16	846	15.9823	1.4	76.8	220.6
cr424 _x			10.4587	-84.6793	7.7	14.5	5/2/7	305	6.9836	3.6	81.8	26.8
cr425 _y			10.7838	-85.4258	184.5	-17.5	4/1/5	269	4.9870	4.8	-85.2	206.6
cr426 _y	CR-025	2032 ± 10 ⁽³⁾	10.4744	-85.0460	173.1	8.8	7/1/8	209	7.9690	3.9	-73.6	300.0
cr427 _x			9.9724	-83.7844	0.1	43.7	8/2/10	598	9.9866	2.0	74.4	276.6
cr428 _y	CR-014B	41 ± 2 ⁽³⁾	10.2594	-84.1769	285.5	5.0	6/1/7	30	6.8147	11.4		
cr429 _x	CR-013	61 ± 2 ⁽³⁾	10.2080	-84.1635	358.8	30.6	6/0/6	469	5.9893	3.1	83.6	265.4
cr430 _x			10.1909	-84.2334	357.1	26.3	6/3/9	718	8.9909	2.0	85.3	238.5
cr431 _y			10.0601	-84.0800	8.2	23.0	3/2/5	2.0	3.3940	79.1		
All			10.1415	-84.3748	2.7	13.1	28	12.5	25.8352	8.0	85.6	58.1
Normal			10.0931	-84.2910	1.7	15.5	24	13.9	22.3402	8.2	87.2	58.2
Reverse			10.4575	-84.8775	188.7	2.0	4	8.9	3.6645	32.5	-75.6	237.5

^aSite names are referred to in this paper. Underlined sites were not included in *Johnson et al.* [2008]. Sites with subscript _x are reinterpreted from the original collection and contain additional samples. Sites with _y are reinterpreted with no additional samples. Alt. Names are referred to in their respective geochronology publications. Dec and Inc are mean site declination and inclination. nl/np is the number of best-fit lines and planes, respectively, nn is the combined number of best-fit lines and planes of all the specimens used in site calculations, (N) is the number of sites used for the average directions of All (reverse directions flipped to normal polarity), Normal and Reverse accepted sites. k_w is an estimate of the Fisher [1953] precision statistic reflecting within site scatter, (k) is an estimate for dispersion for all accepted sites. R is the resultant vector of nn (or N) unit vectors. α_{95} is the Fisher [1953] circle of 95% confidence. VGP Lat and Lon are the virtual geomagnetic poles calculated for each site.

^bAverage ⁴⁰Ar/³⁹Ar radiometric ages are listed with 2 σ error. The associated references are indicated in parentheses: 1, *Alvarado and Gans* [2012]; 2, *Pérez et al.* [2006]; 3, *Alvarado et al.* [2006].

additional ⁴⁰Ar/³⁹Ar age corresponds with site cr404 and was published by *Alvarado et al.* [2006].

4. Paleodirections

[12] We measured directions of the natural remanent magnetization (NRM) for all specimens using either a 2G or CTF cryogenic magnetometer housed in the magnetically shielded room at SIO. At least five specimens per site were magnetically cleaned either by stepwise alternating field (AF) using the Sapphire Instruments SI-4 uniaxial AF

demagnetizer or by thermal demagnetization in SIO-built ovens. In general, thermal demagnetization was carried out until the maximum unblocking temperature was reached (< 5% of the NRM remaining). Examples of typical demagnetization behavior are shown in Figure 2.

[13] A majority of specimens decay in a univectorial fashion to the origin (e.g., Figures 2a and 2b). However, many thermal demagnetization experiments were carried out in conjunction with the IZZI-modified Thellier-Thellier paleointensity experiments [*Tauxe and Staudigel*, 2004; *Yu et al.*, 2004] described in the following section. Most of the directions derived from the zero field

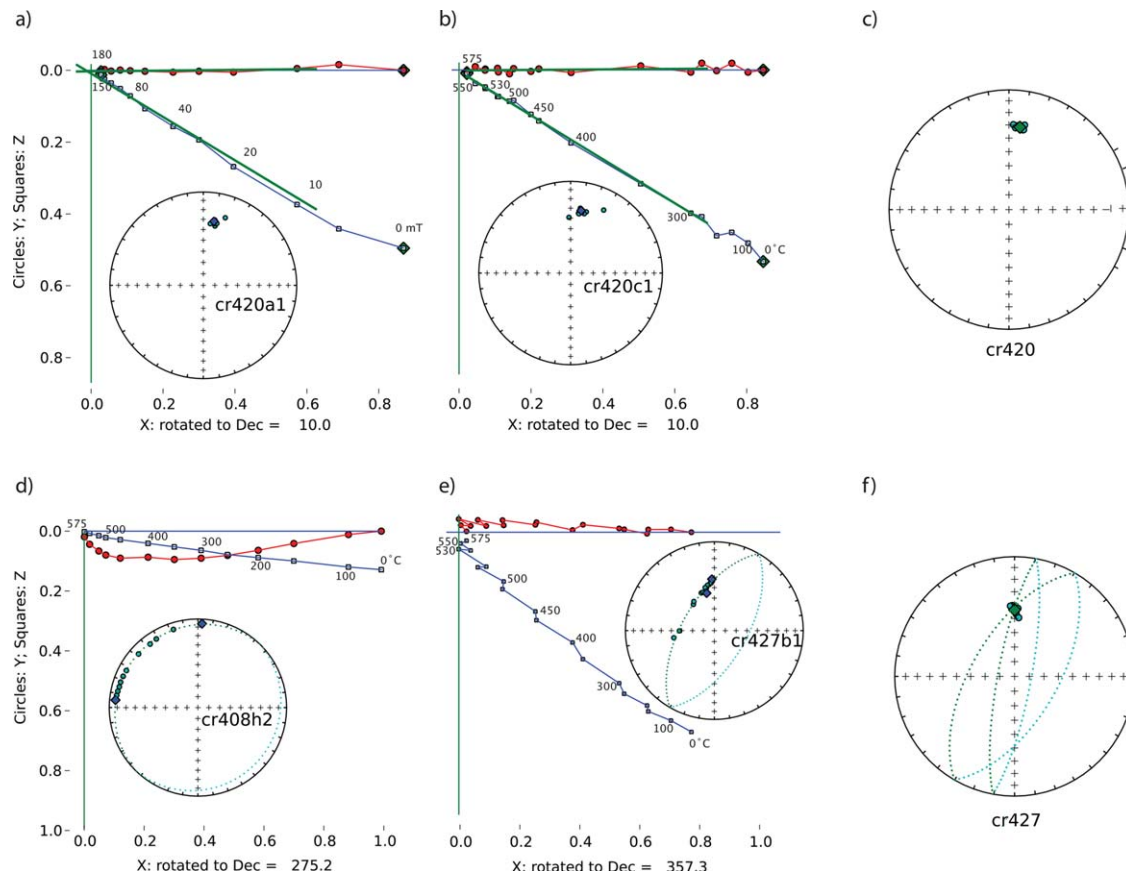


Figure 2. Typical “Type I” site. (a) AF demagnetization shows straightforward, univectorial decay to the origin. Inset is plot of directions from each demagnetization step. (b) Thermal demagnetization of sister specimen is similar to AF demagnetization. Inset same as Figure 2a. (c) Directions of all best-fit lines defining characteristic directions similar to Figures 2a and 2b, site mean is green circle. Typical “Type II” site contains at least one AF or thermal demagnetization specimen with univectorial decay to the origin (e.g., Figures 2a or 2b), and at least one specimen similar to Figures 2d or 2e. (d) Thermal demagnetization displaying multicomponent behavior. Inset shows directions at each demagnetization step plotting as a great circle rather than a best-fit line. (e) Demagnetization derived from Thellier (IZZI) experiment showing contamination from the applied lab field. Inset is the same as Figure 2d. (f) Same as Figure 2c except including great circle fits.

steps (57 in total) show evidence of overprinting in the lab field direction (e.g., Figure 2e). A small number of specimens subject to thermal demagnetization also appear to contain overprints of unknown origin. Some specimens exhibit a behavior termed “gyroremanent magnetization” (GRM) [Stephenson, 1993], where specimens acquire a direction orthogonal to the last demagnetization axis during AF demagnetization. Specimens displaying GRM behavior were excluded from the site mean calculation.

[14] Principal component analysis [Kirschvink, 1980] was used to determine characteristic directions or best-fit planes for each specimen. Generally, univectorial decay was fit with a line while data affected by laboratory overprints like pTRM

acquisition were fit by planes. The assumption is that the original characteristic direction is constrained to lie within the best-fit plane. Specimen lines and planes were deemed acceptable if they had at least four consecutive demagnetization steps and a maximum angle of deviation (MAD) $\leq 5^\circ$.

[15] Our inclusion of new paleodirectional measurements and reanalysis of the original paleomagnetic data from Johnson *et al.* [2008] clarifies the interpretation of two lava flows (cr414 and cr035), although it does not significantly alter the original results. We determined that site cr414 is in fact three separate lava flows (cr414l, cr414m, and cr414u). Field observations note that there is no clear continuous outcropping of site cr414, so

samples were taken from three distinct sections (lower, middle, and upper). Mean directions from each section are distinct from each other according to a statistical bootstrap common mean test [Tauxe, 2010]. We separate cr414 into three distinct cooling units due to the uncertainty in field observations and the unique directions from each section. Sites cr414l and cr414u are included in our new site mean analysis, while cr414m did not meet our site level acceptance criteria ($nn \geq 5$, $k_w \geq 50$). We also determined that the orientation information for samples in site cr035 was incorrectly transcribed from the field notebook during initial processing. Site cr035 now passes all selection criteria with correct orientation information. cr035 is the same lava flow as cr405 but we only use site cr405 in our site mean analysis, rather than combining cr035 and cr405, because demagnetized samples from cr405 (7/10) are predominantly univectorial and contain no overprints (compared to 1/11 for cr035). All other sites are essentially unchanged from the original publication of Johnson *et al.* [2008]. In total, the revised data set contains 28 acceptable paleodirectional sites from 35 sampled lavas. Five sites fail our site level criteria (cr414m, cr416, cr421, cr428, and cr431) and two sites were determined to be the same lava flow (cr422 and cr423) and combined.

[16] Two types of site level demagnetization behavior were observed (Figure 2). Type I sites (10 total) decayed linearly to the origin in both AF and thermal demagnetization experiments (e.g., Figures 2a and 2b). Type II sites (20 total) were characterized by some specimens exhibiting laboratory overprints (e.g., Figures 2d and 2e). Site means for Type I sites (Figure 2c) were calculated using Fisher statistics [Fisher, 1953] and the combined lines and planes method of McFadden *et al.* [1988] was used for Type II sites (Figure 2f).

[17] Figure 3 shows equal area plots of site mean directions (Figure 3a) and orthographic plots of site virtual geomagnetic poles (VGPs) (Figure 3b). The average of all site mean directions are consistent with that expected from a geocentric axial dipole (GAD) field (yellow star) (see Table 1). Reverse polarity sites are antipodal to normal sites and the data pass Watson's V_w test [Tauxe, 2010].

[18] Cox [1969] routinely used the angular standard deviation of VGPs about the geographic pole as a measure of the paleosecular variability of the paleomagnetic field. Detailed age information for each VGP is not required provided the temporal sampling is adequate. The total scatter statistic S

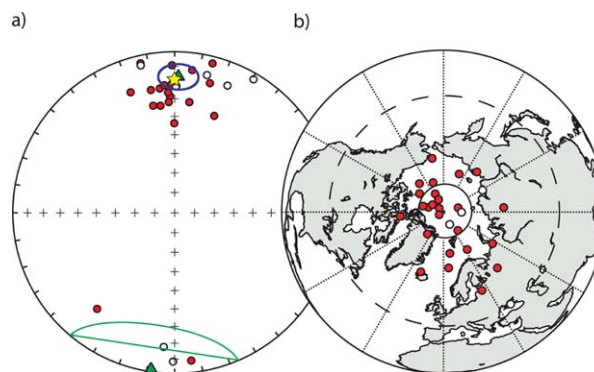


Figure 3. (a) Equal area projection of site-mean directions meeting site level selection criteria. Filled circles are positive inclinations and plot in the lower hemisphere, open circles are negative inclinations and plot in the upper hemisphere. Mean directions (green triangles) with Fisher a95 confidence cones for normal (blue circle) and reversed (green circle) sites. Yellow star is the expected direction from a GAD field. (b) VGP positions for all accepted directional sites. Filled (open) circles are positive (reversed, anti-podal) VGP positions. Dashed circle is at 45° latitude.

specified by Cox [1969] is modified to correct for the within-site directional scatter S_w [McElhinny and McFadden, 1997] and the statistic S_F is now commonly used.

$$S_F = \sqrt{(N-1)^{-1} \sum_{i=1}^N \left((\Delta_i)^2 - \frac{S_w^2}{nn_i} \right)}, \quad (1)$$

where N is the total number of sites, Δ_i is the angle between the i th VGP and the spin axis, S_w is within-site scatter (defined as $81^\circ / \sqrt{k_w}$, where k_w is the within-site Fisherian precision statistic), and nn_i is the number of samples from the i th site.

[19] In Table 2, we list S_F for Costa Rica with no cutoff, a variable colatitude cutoff specified according to the normal secular variations criteria of Vandamme [1994] and a 45° cutoff. Our revised calculation of unfiltered VGP dispersion (with 95% confidence) in Costa Rica is $17.3_{12.8}^{21.9}$ and remains essentially unchanged from prior publication of the data in Johnson *et al.* [2008], $17.5_{12.5}^{22.5}$. Our recalculation of VGP dispersion is within error of the predicted dispersion from the PSV model TK03 [Tauxe and Kent, 2004], which predicts VGP scatter of $15.6_{15.1}^{16.0}$ at 10° latitude.

5. Paleointensity

[20] We used the IZZI-modified Thellier-Thellier experiment [Tauxe and Staudigel, 2004] to



Table 2. VGP Scatter, S_F , With Bootstrapped 95% Confidence Bounds^a

Lat	N_F	S_F	N_{F_V}	S_{F_V}	$N_{F_{45}}$	$S_{F_{45}}$
10.1°	28	17.3 ^{21.9°} _{12.8}	27	15.2 ^{18.2°} _{11.9}	27	15.2 ^{18.3°} _{12.1}

^aLat is the average location latitude, N is number of sites used to calculate VGP scatter using no colatitudinal cutoff, S_F , the iterative cutoff of Vandamme [1994], S_{F_V} , and a 45° cutoff, $S_{F_{45}}$. The calculated colatitudinal cutoff for S_{F_V} is 32.0°.

estimate paleointensity. All paleointensity experiments were performed in the magnetically shielded room at SIO using custom-built ovens. In the IZZI method, the specimens are heated in alternating zero-field and in-field temperature steps in order to detect inequalities in blocking and unblocking temperature which is characteristic of certain non-single domain populations.

[21] There is evidence to suggest that the intensity of the laboratory field in Thellier-Thellier paleointensity

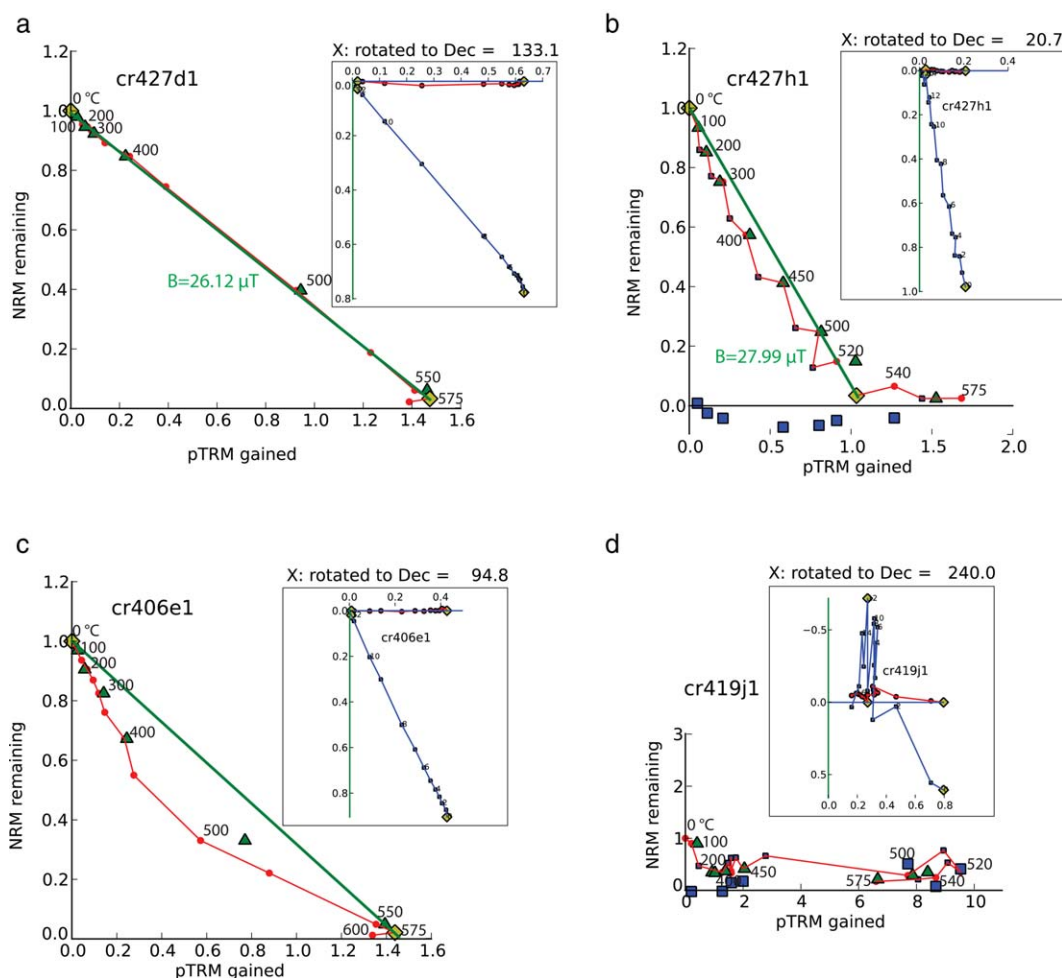


Figure 4. Arai plots of NRM remaining versus pTRM gained during IZZI-modified Thellier-Thellier paleointensity experiments for select specimens. Red circles (blue squares) represent ZI (IZ) heating steps. The green line is the estimated paleointensity component with the accompanying intensity value. pTRM checks are shown as small green triangles and pTRM tail checks are large blue squares. Insets are vector-endpoint (Zijderveld) diagrams, where the x -axis has been rotated to the mean NRM direction. Circles (squares) are the horizontal (vertical) plane. Yellow diamonds represent the bounds used in principal component analysis. (a) cr427d1 (NRM normalized to $3.53 \times 10^{-5} Am^2$) is an ideally behaved specimen with a linear Arai plot encompassing the entire TRM, (b) cr427h1 ($1.21 \times 10^{-5} Am^2$) appears to be multidomain, however we accept this specimen because the nonlinear behavior is most likely a result of alteration and occurs after meeting all specimen level criteria (see text), (c) cr406e1 ($3.60 \times 10^{-5} Am^2$), multidomain-like specimen rejected because no linear component can be derived (see text), and (d) cr419j1 ($1.81 \times 10^{-6} Am^2$) fails all pTRM checks and no intensity component can be derived.



Table 3. Paleointensity Results for Costa Rica^a

Site	nn_B	$B(\mu\text{T})$	σ_B	$d\sigma_B$	VADM ($\times 10^{22}$ Am ²)	σ_{VADM}	VDM ($\times 10^{22}$ Am ²)
cr418	3	25.5	3.75	14.7	63.0	9.26	65.5
cr427	2	27.1	1.32	4.9	67.0	3.26	56.1
Specimen Criteria		Definition					
$f_{\text{vds}} \geq 0.7$		Fraction of the Total Remanence (by vector difference sum)					
$\text{MAD} \leq 5$		Maximum angle of deviation					
$\text{DRATS} \leq 20$		Difference ratio sum					
$\text{DANG} \leq 10^\circ$		Deviation of the angle					
$\text{MD}\% \leq 15\%$		Maximum difference percent					
$Z \leq 4$		Zig-Zag					
$\beta \leq 0.1$		"Scatter" parameter					

^a nn_B is the number of specimens used in paleointensity calculation. B (μT) is the average field strength at each site. σ_B is the standard deviation of the specimens used to calculate the site mean. $d\sigma_B$ is the standard deviation of the specimen intensities as a percent fraction of the mean intensity. VADM is the virtual axial dipole moment and σ_{VADM} is the standard deviation of specimens used to calculate the mean VADM. Below are specimen level and site level acceptance criteria. See *Tauxe* [2010] for a description of all criteria definitions.

experiments, and its derivatives, has no influence on the ability to recover the ancient magnetic field strength [e.g., *Morales et al.*, 2006]. Other studies observe that the success of the IZZI-modified method is dependent on the strength and direction of the applied lab field relative to the ancient NRM of the specimen [*Yu et al.*, 2004; *Shaar et al.*, 2011]. Empirical experiments by *Shaar et al.* [2011] suggest that the best overall performance of the IZZI method for recovering the ancient field, regardless of applied field angle, is when the laboratory field strength is equal to or less than the ancient field strength. In our IZZI experiments, the NRM directions of our specimen cores are randomly oriented in the oven; therefore, we applied lab fields of 30 and 40 μT in an attempt to approximate the expected ancient field strength. All experiments were carried out to 600°C or until at least 95% of the NRM was demagnetized.

[22] Figure 4 shows examples of Arai plots [*Nagata et al.*, 1963] from representative IZZI experiments. Insets are Zijderveld diagrams [*Zijderveld*, 1967] plotting the behavior of the remanence (zero-field steps). We only accept ideally behaved specimens (Figure 4a) that plot as straight lines in the Arai plots, with no evidence of alteration (pTRM checks plot on top of initial pTRM measurements) or multicomponent behavior in the Zijderveld diagrams. We exclude specimens that exhibit concave-up Arai plots (Figure 4c) and specimens that acquired a remanence parallel to the laboratory field which is not demagnetized by later heating steps (Figure 4d).

[23] We screen out specimens that exhibit alteration or contain multicomponent remanences, by using the following strategy (see Table 3 for criteria definitions): (1) Each specimen must have a relatively linear component of magnetization representing a majority of the TRM applied to

the specimen ($f_{\text{vds}} \geq 0.7$) with a $\text{MAD} \leq 5$; (2) no data can be used at temperature steps greater than a failed pTRM check as defined by a DRAT of 20%; (3) the temperature range of the interpreted intensity component must be related to the characteristic remanent magnetization of the specimen ($\text{DANG} \leq 10^\circ$); and (4) no temperature step may be used where the pTRM gained is lower than the gain of the previous temperature step.

[24] At the site level, we require at least two intensity estimates per site, $nn_B \geq 2$, and evaluate the percent standard deviation of the mean intensity, which is $d\sigma_B = 100 \times \sigma_B / B$. We use a $d\sigma_B$ cutoff of 15% in order to ensure that large outliers do not adversely effect the final paleointensity estimation.

[25] Despite our reluctance to include specimens that display concave-up Arai plots, we made an exception for specimen cr427h1 (Figure 4b) where we determined that the observed behavior was not likely multidomain. The linear segment of the Arai plot passes all specimen level criteria (1–4) and the concave-up portion occurs after a failed pTRM check, indicating that high temperature alteration is a plausible cause of this behavior. It can be assumed that if alteration did not occur then the slope of the intensity component would remain linear through the remainder of the IZZI experiment. If our interpretation is incorrect and the observed behavior in this specimen is not caused by alteration, then the low-temperature components we selected would likely overestimate the ancient magnetic field strength.

[26] Two of our 34 sampled lava flows meet all the above criteria, cr418 and cr427 (see Table 3). The two sites have an average paleointensity of



26.3 μT and a virtual axial dipole moment (VADM) of 65 ZAm^2 . These estimates are lower than present day Costa Rica values (35.3 μT and 87 ZAm^2), but are well within the range of published paleointensity results from similar latitudes (as compiled in the PINT10.12 database [Biggin et al., 2010]) and within one standard deviation (15 ZAm^2) of the 0–2 Ma average paleomagnetic axial dipole moment of 53 ZAm^2 found from a comprehensive analysis by Ziegler et al. [2011].

6. Conclusions

[27] We present here a comprehensive report on our paleomagnetic study of Plio-Pleistocene lavas from Costa Rica. Preliminary results from this study were published by Johnson et al. [2008] as part of the TAFI project. New directional and paleointensity analysis of volcanic sites from Costa Rica produce 28 high-quality directional sites and two paleointensity estimates with $^{40}\text{Ar}/^{39}\text{Ar}$ geochronology ages ranging from 41 ka to 6.1 Ma. Unfiltered VGP dispersion for 28 directional sites ($17.3_{12.8}^{21.9^\circ}$) is consistent with PSV predictions of model TK03. Average paleointensity (26.3 μT) and VADM (65 ZAm^2) are within range of paleointensity estimates from similar latitudes. This study contributes to the body of TAFI publications and is a valuable contribution to the paleomagnetic database because of the addition of low-latitude directional and intensity sites.

[28] The full data set including measurements, interpretations, site mean directions, VGPs, and VADMs will be made public in the MagIC database. To access these data, go to <http://earthref.org/MAGIC>.

Acknowledgments

[29] We thank Guillermo Alvarado and Wendy Perez for assistance with field logistics in Costa Rica, and Jason Steindorf for his contributions to sample preparation and processing. Many thanks to Laurie Brown and one anonymous reviewer for their constructive and helpful comments. This material is based on work supported by National Science Foundation grants EAR1141840 to LT and EAR0809709 to CGC.

References

Alvarado, G., and P. Gans (2012), Síntesis geocronológica del magmatismo, metamorfismo y metalogenia de Costa Rica, América central, *Rev. Geol. Am. Cent.*, *46*, 7–122.

- Alvarado, G., M. Carr, B. Turrin, C. Swisher, III, H.-U. Schmincke, and K. Hudnut (2006), Recent volcanic history of Irazú volcano, Costa Rica: Alternation and mixing of two magma batches, and pervasive mixing, *Geol. Soc. Am., Spec. Pap.*, *412*, 259–276, doi:10.1130/2006.2412(14).
- Biggin, A., A. McCormack, and A. Roberts (2010), Palaeointensity database updated, *Eos Trans. AGU*, *91*, 15.
- Constable, C., and R. L. Parker (1988), Statistics of the geomagnetic secular variation for the past 5 m.y., *J. Geophys. Res.*, *93*, 11,569–11,581, doi:10.1029/JB093iB10p11569.
- Cox, A. (1969), Research note: Confidence limits for the precision parameter, *Geophys. J. R. Astron. Soc.*, *17*, 545–549, doi:10.1111/j.1365246X.1969.tb00257.x.
- Drummond, M., M. Bordelon, J. Debor, M. Defant, H. Bellon, and M. Feigenson (1995), Igneous petrogenesis and tectonic setting of plutonic and volcanic rocks of the Cordillera de Talamanca, Costa Rica-Panama, Central American Arc, *Am. J. Sci.*, *295*(7), 875–919.
- Fisher, R. A. (1953), Dispersion on a sphere, *Proc. R. Soc. London, Ser. A*, *217*, 295–305, doi:10.1098/rspa.1953.0064.
- Gans, P., I. MacMillan, G. Alvarado-Inundi, W. Perez, and C. Sigaran (2002), Neogene evolution of the Costa Rican Arc, *Geol. Soc. Am. Abstr. Programs*, *224*(12), 74.
- Hulot, G., and J. Le Mouél (1994), A statistical approach to the Earth's main magnetic field, *Phys. Earth Planet. Inter.*, *82*, 167–183, doi:10.1016/0031-9201(94)90070-1.
- Johnson, C. L., and C. G. Constable (1995), The time-averaged geomagnetic field as recorded by lava flows over the last 5 Myr, *Geophys. J. Int.*, *122*, 489–519, doi:10.1111/j.1365-246X.1995.tb07010.x.
- Johnson, C. L., et al. (2008), Recent investigations of the 0–5 Ma geomagnetic field recorded in lava flows, *Geochem. Geophys. Geosyst.*, *9*, Q04032, doi:10.1029/2007GC001696.
- Kirschvink, J. L. (1980), The least-squares line and plane and the analysis of paleomagnetic data, *Geophys. J. R. Astron. Soc.*, *62*, 699–718, doi:10.1111/j.1365246X.1980.tb02601.x.
- Lee, S. (1983), A study of the time-averaged paleomagnetic field for the past 195 million years, PhD Thesis, Aust. Natl. Univ., Canberra.
- MacMillan, I., P. Gans, and G. Alvarado (2004), Middle Miocene to present plate tectonic history of the southern Central American Volcanic Arc, *Tectonophysics*, *392*, 325–348, doi:10.1016/j.tecto.2004.04.014.
- McElhinny, M. W., and P. L. McFadden (1997), Palaeosecular variation over the past 5 Myr based on a new generalized database, *Geophys. J. Int.*, *131*, 240–252, doi:10.1111/j.1365-246X.1997.tb01219.x.
- McElhinny, M. W., and R. T. Merrill (1975), Geomagnetic secular variation over the past 5 m.y., *Rev. Geophys. Space Phys.*, *13*, 687–708.
- McElhinny, M. W., P. L. McFadden, and R. T. Merrill (1996), The time-averaged paleomagnetic field 0–5 Ma, *J. Geophys. Res.*, *101*, 25,007–25,027, doi:10.1029/96JB01911.
- McFadden, P. L., R. T. Merrill, and M. W. McElhinny (1988), Dipole/Quadrupole family modeling of paleosecular variation, *J. Geophys. Res.*, *93*, 11,583–11,588, doi:10.1029/JB093iB10p11583.
- Morales, J., A. Goguitaichvili, L. Alva-Valdivia, and J. Urrutia-Fucugauchi (2006), Further details on the applicability of Thellier paleointensity method: The effect of magnitude of laboratory field, *C. R. Geosci.*, *338*, 507–513, doi:10.1016/j.crte.2006.02.007.
- Nagata, T., Y. Arai, and K. Momose (1963), Secular variation of the geomagnetic total force during the last 5000 years, *J. Geophys. Res.*, *68*, 5277–5282.



- Pérez, W., G. Alvarado, and P. Gans (2006), The 322 ka Tiríbi Tuff: Stratigraphy, geochronology and mechanisms of deposition of the largest and most recent ignimbrite in the Valle Central, *Costa Rica, Bull. Volcanol.*, *69*, 25–40, doi:10.1007/s00445-006-0053-x.
- Sadalmelik (2007), Topographic map of Costa Rica, Wikimedia Commons.
- Shaar, R., H. Ron, L. Tauxe, R. Kessel, and A. Agnon (2011), Paleomagnetic intensity derived from non-SD: Testing the Thellier IZZI technique on MD slag and a new bootstrap procedure, *Earth Planet. Sci. Lett.*, *310*(3–4), 213–224, doi:10.1016/j.epsl.2010.11.013.
- Stephenson, A. (1993), Three-axis static alternating field demagnetization of rocks and the identification of NRM, gyroremanent magnetization, and anisotropy, *J. Geophys. Res.*, *98*, 373–381, doi:10.1029/92JB01849.
- Tauxe, L. (2010), *Essentials of Paleomagnetism*, p. 489, Univ. of Calif. Press, Berkeley, Calif.
- Tauxe, L., and D. V. Kent (2004), A simplified statistical model for the geomagnetic field and the detection of shallow bias in paleomagnetic inclinations: Was the ancient magnetic field dipolar?, in *Timescales of the Paleomagnetic Field*, vol. 145, edited by J. E. T. Channell, et al., pp. 101–116, AGU, Washington, D. C.
- Tauxe, L., and H. Staudigel (2004), Strength of the geomagnetic field in the Cretaceous Normal Superchron: New data from submarine basaltic glass of the Troodos Ophiolite, *Geochem. Geophys. Geosyst.*, *5*, Q02H06, doi:10.1029/2003GC000635.
- Vandamme, D. (1994), A new method to determine paleosecular variation, *Phys. Earth Planet. Int.*, *85*, 131–142, doi:10.1016/0031-9201(94)90012-4.
- Vogel, T., L. Patino, G. Alvarado, and P. Gans (2004), Silicic ignimbrites within the Costa Rican Volcanic front: Evidence for the formation of continental crust, *Earth Planet. Sci. Lett.*, *226*, 149–159, doi:10.1016/j.epsl.2004.07.013.
- Yu, Y., L. Tauxe, and A. Genevey (2004), Toward an optimal geomagnetic field intensity determination technique, *Geochem. Geophys. Geosyst.*, *5*, Q02H07, doi:10.1029/2003GC000630.
- Ziegler, L., C. Constable, C. L. Johnson, and L. Tauxe (2011), PADM2M: A penalized maximum likelihood model of the 0–2 Ma palaeomagnetic axial dipole moment, *Geophys. J. Int.*, *184*, 1069–1089, doi:10.1111/j.1365-246X.2010.04905.x.
- Zijderveld, J. (1967), A.C. demagnetization of rocks: Analysis of results, in *Methods in Paleomagnetism*, edited by D. W. Collinson, K. M. Creer, and S. K. Runcorn, pp. 254–286, Amsterdam.
- Zimmer, M., T. Fischer, D. Hilton, G. Alvarado, Z. Sharp, and J. Walker (2004), Nitrogen systematics and gas fluxes of subduction zones: Insights from Costa Rica arc volatiles, *Geochem. Geophys. Geosyst.*, *5*, Q05J11, doi:10.1029/2003GC000651.